

NASA-CR-199438

*P. 20*  
*1N-34-CR*  
*5027*

UNIVERSITY OF CINCINNATI

FINAL REPORT

HIGH SPEED NOZZLES TASK

**Awatef Hamed**  
**Principal Investigator**

OAI Subcontract No. 120520  
27 September 1993 - 26 June 1995

N96-10873

Unclas

G3/34 0068092

Submitted to

**Dr. Robert J. Shaw, Project Monitor**  
**NASA Lewis Research Center, MS AAC-1**  
**12000 Brookpark Avenue**  
**Cleveland, OH 44135**

September 7, 1995

(NASA-CR-199438) HIGH SPEED  
NOZZLES TASK Final Report, 27 Sep.  
1993 - 26 Jun. 1995 (Cincinnati  
Univ.) 26 p

## TABLE OF CONTENTS

ABSTRACT .....	1
INTRODUCTION .....	1
ANALYSIS .....	2
SUMMARY OF THE RESULTS .....	3
CONCLUSIONS .....	3
REFERENCES .....	4
APPENDIX A .....	6
APPENDIX B .....	15

# INLETS AND NOZZLES RFP HIGH SPEED NOZZLES TASK

## Abstract

Supersonic cruise exhaust nozzles for advanced applications are optimized for a high nozzle pressure ratio (NPR) at design supersonic cruise Mach number and altitude. The performance of these nozzles with large expansion ratios are severely degraded for operations at subsonic speeds near sea level for NPR significantly less than the design values. The prediction of over-expanded 2DCD nozzles performance is critical to evaluating the internal losses and to the optimization of the integrated vehicle and propulsion system performance. The reported research work was aimed at validating and assessing existing computational methods and turbulence models for predicting the flow characteristics and nozzle performance at over-expanded conditions. Flow simulations in 2DCD nozzles were performed using five different turbulence models. The results are compared with the experimental data for the wall pressure distribution and thrust and flow coefficients at over-expanded static conditions.

## Introduction

Recent technological advances in gas turbine engine materials, structures, cooling techniques, and analytical and computational tools, have resulted in considerable weight reductions and performance improvements. With these general advancements, and the variable cycle engine technology development through the NASA sponsored AST program, the viability of supersonic transport above Mach 2 appears to be reasonable in the early 2000's[1]. In the exhaust nozzle system, innovative structural designs and cooling techniques are required because of the higher pressures, temperatures and the large required changes in the nozzle area ratio for performance optimization at off-design conditions [2].

The nozzle design requirements are dictated by the aircraft performance and operational requirements as well as the engine cycle aerothermodynamics and operational characteristics. In general, the nozzle pressure ratio, NPR, and area ratio, AR, increase sharply with design point flight Mach number [3, 4]. While sustained high Mach number operation requires high nozzle area ratio for best efficiency at supersonic cruise, the lower area ratios required at subsonic acceleration (off design conditions) might not be achievable because of mechanical and control system constraints. Under these conditions, the nozzle will operate over-expanded with a consequent loss in the thrust coefficient due to the occurrence of compression shocks inside the nozzle, accompanied by flow separation from the nozzle wall. The poor performance of the De Laval nozzle at pressure ratios below the design values has led to the development of plug nozzles [5-7] and ejector nozzles [8, 9]. Plug nozzles offer the advantage of short length while ejector nozzles contribute to the overall performance when air pumping is required for internal cooling. In optimizing the overall performance of the exhaust nozzle system, the boattail or external drag should be considered together with the internal losses consisting of friction, angularity, leakage and

expansion losses. The maximum installed performance usually occurs at a larger area ratio than that required to optimize the internal performance [2].

When a convergent divergent nozzle operates over-expanded, the pressure waves from the higher back pressure can only propagate upstream through the subsonic flow regions of the boundary layer. If the back pressure is slightly higher than the nozzle flow exit static pressure, oblique shock waves form at the corner of the exit section and the flow is compressed to the back pressure by flowing through the shocks. If the difference between the back pressure and the exit static pressure increases the flow separates on the nozzle's divergent wall. Stodola [10] was the first to report static pressure distribution curves in an over-expanded De Laval nozzle. Subsequent measurements in over-expanded rocket motor nozzles indicated that for a given nozzle divergence angle, the separation pressure ratio is a function of the NPR [11]. According to reference [2], two percent reduction in the thrust coefficient will reduce the net thrust by 12-16% at Mach 4 flight conditions. The accurate prediction of the flow field in general and the separation point in particular is critical to calculating the thrust and flow coefficients, and the nozzle cooling flow characteristics.

Nozzle flow fields at over-expanded flow conditions are complicated by shock-wave/boundary-layer interactions, flow separation and mixed subsonic and supersonic conditions at the nozzle exit. Depending on the nozzle pressure ratios NPR, the shocks can be contained within the divergent passage or the shock structure can extend outside the nozzle exit. The performance loss as measured by the thrust coefficient will be greater in the case of flow separation due to the shock system within the nozzle which is the configuration emphasized in the present study. When the NPR are high but still lower than the design pressure ratio, the shock structure consists of oblique shocks originating at the nozzle exit and perhaps a normal shock in the central region. In order to study the nozzle flow in this case, it is necessary to include the external flow field into the simulations [12, 13]. When the NPR is sufficiently low, the shock structure consisting of a normal shock at the center and a Lambda or oblique shock near the walls reside in the nozzle divergent passage and the flow simulations under static conditions need be performed only within the nozzle (internal flow field simulations). Under these circumstances, the fidelity in simulating the shock induced flow separation is key to the accuracy of nozzle performance predictions.

## Analysis

Numerical simulations were conducted for the compressible Navier-Stokes equations in general curvilinear coordinates and conservation law form to accurately capture the Rankine-Hugoniot shock jump conditions. Five different turbulence closure models were assessed, including two algebraic [14], one one-equation [15] and two two-equation models [16, 17]. An implicit solver was used to advance the time dependent governing equations to steady state conditions, using local time stepping as dictated by the maximum allowable CFL number.

The computations were performed using the PARC code [18] which was developed at Arnold Engineering Development Center (AEDC) and is now the national PARC code (NPARC) supported by NASA Lewis Research Center and AEDC. The code incorporates several algorithms for the solution of the Navier-Stokes equations in strong conservation law form. The Pulliam's diagonalized algorithm that employs an implicit LU-ADI style solver was used to obtain a steady state solution.

In the nozzle flow simulations, the total pressure and temperature are prescribed at the upstream boundary, no slip adiabatic wall conditions are specified at the nozzle walls, and the static pressure at the downstream boundary.

### Summary of the Results

Validation cases were selected from existing experimental data [19, 20] for two dimensional nonaxisymmetric nozzles which were tested in the static test facility of Langley's 16-ft. transonic tunnel. The computational grid was generated using GRIDGEN [21] code, and a grid refinement study was conducted to select the appropriate grid size. The computations were performed for two 2D-CD nozzle geometries with high divergence angles corresponding to a design pressure ratio of 8.8 and an exit Mach number of 2.1. The computational results were compared with the experimental data over a wide range of nozzle pressure ratios (1.8-8.8), corresponding to overexpanded conditions. The detailed results were presented in the following two publications:

1. "Performance Prediction of Overexpanded 2DCD Nozzles," by A. Hamed, C. Vogiatzis and J.J. Yeuan, 12th Int. Symposium on Air Breathing Engines, September 10-15, 1995, Melbourne, Australia (Appendix A).
2. "Assessment of Turbulence Models in Overexpanded 2D-CD Nozzle Flow Simulations," by A. Hamed and C. Vogiatzis, 31st AIAA/ASME/SAE/ASEE Joint Propulsion Conference and Exhibit, July 1995, San Diego, CA (Appendix B).

### Conclusions

At the design nozzle pressure ratio, all the computational results were in excellent agreement with the experimental static pressure distribution and thrust coefficient. At the low pressure ratios corresponding to overexpanded flow conditions with shocks inside the nozzle, the computed wall pressure distribution using the two equation turbulence models were the closest to the experimental results. The other turbulence models either did not predict accurately the shock location, or the pressure rise in the separation region. The computational results agreement with the experimental data was much better for higher pressure ratios and less accurate for the lower nozzle pressure ratios. The inclusion of the region external to the nozzle into the numerical solution to simulate the interactions between the external flow and the flow inside the nozzle in the recirculation regions did not improve the prediction of the thrust coefficient at the low nozzle pressure ratios.

The results indicate that the two dimensional flow simulations can predict the nozzle thrust coefficient within 1% of the experimental data at nozzle pressure ratios greater than or equal to half the design pressure ratio, but that three dimensional effects should be simulated for better flow predictions at lower nozzle pressure ratios.

### References

1. Shaw, R.J., Gilkey, S. and Hines, R., "Engine Technology Challenges for a 21st Century High-Speed Civil Transport," NASA TM 106216, September 1993.
2. Dusa, D.J., "Exhaust Nozzle System Design Considerations for Turboramjet Propulsion Systems," ISOABE Ninth International Symposium on Air Breathing Engines, Athens, Greece, September 1989.
3. Flugstad, T.H., Romine, B.M. and Whittaker, R.W., "High Mach Exhaust System Concept Scale Model Test Results," AIAA Paper 90-1905, July 1990.
4. Kuchar, A.P. and Wolf, J.P., "Preliminary Assessment of Exhaust Systems for High Mach (4 to 6) Fighter Aircraft," AIAA Paper 89-2356, July 1989.
5. Berman, K., and Crimp, F.W., "Performance of Plug-Type Rocket Exhaust Nozzles," ARS Journal, Vol. 31, No. 1, January 1961.
6. Hearth, D.P., and Gorton, G.C., "Investigation of Thrust and Drag Characteristics of a Plug-Type Exhaust Nozzle," NACA RM E53L16, 1954.
7. Berrier, B.L., "Effect of Plug and Shroud Geometry Variables on Plug-Nozzle Performance at Transonic Speed," NASA TND-5098, March 1969.
8. Huntley, S.C., and Yanowitz, H., "Pumping and Thrust Characteristics of Several Divergent Cooling Air Ejectors and Comparison of Performance with Conical and Cylindrical Ejectors," NACA E53J13, 1953.
9. Luffy, R.J., and Hamed, A., "A Study on the Impact of Shroud Geometry on Ejector Nozzle performance," AIAA Paper 92-3260, 28th Joint Propulsion Conference and Exhibit, Nashville Tennessee, July 1992.
10. Stodola and Loewenstein, "Steam and Gas Turbines," Peter Smith, 1945.
11. Green, L., "Flow Separation in Rocket Nozzle," J. ARS, January-February 1953, p.34.
12. Carlson, J.R. and Abdol-Hamid, K.S., "Prediction of Static Performance for Single Expansion Ramp Nozzles," AIAA Paper 93-2571, June 1993.
13. Carlson, J.R. and Pao, S.P., "Computational Analysis of Vented Supersonic Exhaust Nozzles Using a Multiblock/Multizone Strategy," AIAA 91-0125, January 1991.
14. Baldwin, B.S., Lomax, H., "Thin-Layer Approximation and Algebraic Model for Separated Turbulent Flows," AIAA Paper 78-257, January 1978.
15. Baldwin, B.S., Barth, T.J., "A One-Equation Turbulence Transport Model for High Reynolds Number Wall-Bounded Flows," NASA-TM-102847, August 1990, N91-10252.

16. Chien, K-Y, "Prediction of Channel and Boundary-Layer Flows with a Low Reynolds Number Turbulence Model," AIAA Journal, Vol. 20, January 1982, pp. 33-38.
17. Wilcox, D.D., "The Remarkable Ability of Turbulence Model Equations to Describe Transition," 5th Symposium on Numerical and Physical Aspects of Aerodynamic Flows, California State University, Long Beach, CA, 13-15 January 1992.
18. Cooper, G.K., and Sirbaugh, J.R., "PARC Code: Theory and Usage," AEDC-TR-89-15, 1989.
19. Mason, M.L., Putnam, L.E. and Re, R.J., "The Effect of Throat Contouring on Two-Dimensional Converging-Diverging Nozzles at Static Conditions," NASA TP 1704, August 1980.
20. Hunter, C.A., "An Experimental Analysis of Passive Shock-Boundary Layer Interaction Control for Improving the Off-Design Performance of Jet Exhaust Nozzles," M.S. Thesis, George Washington University, September 1993.
21. Steinbrenner, J.P., Chawner, J.R. and Fouts, C.L., "The GRIDGEN 3D Multiple Block Grid Generation System," WRDC-TR-90-3022, Vols I and II. Wright Patterson AFB, OH, 1990.

**APPENDIX A**

## PERFORMANCE PREDICTION OF OVEREXPANDED 2DCD NOZZLES

A. Hamed, C. Vogiatzis and J.J. Yeuan  
University of Cincinnati  
Cincinnati, OH 45221

### Abstract

A numerical investigation of the performance of overexpanded 2DCD nozzles is conducted based on the implicit numerical solution of the compressible Navier-Stokes equations in conservative law form and general curvilinear coordinates. Different turbulence models are assessed in terms of their ability to predict the shock induced flow separation and the associated loss in nozzle performance. In addition, the effect of external flow and its interaction with the large separation regions at the nozzle exit is investigated. The numerical predictions are compared with existing experimental data for the pressure distribution over the flaps and side walls, internal thrust ratios, and discharge coefficients in two nozzle geometries over a range of overexpanded pressure ratios.

### Introduction

Recent advances in engine materials, structures, cooling techniques, and variable cycle engine technology support the development of supersonic transport above Mach 2. While sustained high Mach number operation requires high nozzle area ratio for best efficiency at supersonic cruise, the lower area ratios required at subsonic acceleration might not be achievable because of mechanical and control system constraints [1]. Under these conditions, the nozzle will operate overexpanded with a consequent loss in the thrust coefficient due to the occurrence of compression shocks inside the nozzle, accompanied by flow separation from the nozzle walls.

At overexpanded flow conditions, the shocks can be contained within the divergent passage or they can extend outside the nozzle exit, depending on the nozzle pressure ratio, NPR. At sufficiently low NPR, the shock structure consisting of a normal shock at the center and a lambda shock near the walls reside in the nozzle divergent passage. When the NPR is high but still lower than the design pressure ratio, the shock structure consists of oblique shocks originating at the nozzle exit and perhaps a normal shock in the central region. The performance loss as measured by the thrust coefficient and flow or discharge coefficient is greater in the first

case, since there is a large shock induced flow separation that extends to the nozzle exit.

Recently, several experimental and computational studies have been conducted to evaluate the performance of ejector nozzles [2-4], nozzles with chute suppressors [5] and the drag of conventional nozzles [6]. Few experimental studies however reported results for overexpanded 2DCD nozzles with large recirculation regions [7, 8]. Mason et al. [7] presented internal performance data for five two-dimensional nozzle geometries which were tested at pressure ratios up to 9.0 in the static test facility of Langley's 16-ft transonic tunnel. The nozzle performance data were reported for the 2DCD nozzles/geometries with different divergence angles and throat radii at fourteen nozzle pressure ratios corresponding to design and overexpanded conditions. The data consist of static pressure distributions over the flaps and side walls, internal thrust ratios and discharge coefficients. A second nozzle configuration C2, which has the same design pressure ratio and area ratio as nozzle B2 of reference [7], but smaller throat radius of curvature was tested by Hunter [8] in the same facility. His test results at overexpanded conditions indicate that the flow separates from the flap under the lambda foot of the normal shock, and remains detached until the exit. The extent of flow separation increased with the reduction in the nozzle pressure ratio, as the normal shock moves closer to the throat.

Shieh [9] compared his computational results with the experimental data of Mason et al. [7] at one overexpanded pressure ratio. However, his predicted pressure distributions were not in good agreement with the experimental results in the divergent part of the nozzle. Unlike the experimental data, they depicted a gradual pressure increase in the aft part of the divergent nozzle, did not exhibit the large pressure gradient across the shock, and underpredicted the vena contracta effect at overexpanded flow conditions. The ability to predict the shock location and the extent of flow separation is critical to the computational accuracy of nozzle performance. The onset of flow separation and the extent of separated flow region in shock induced flow separation were found to be affected by turbulence

models and numerical algorithms [10]. In the present investigation, 2DCD nozzle flow field predictions are compared with the experimental data of Mason et al. [7] and Hunter [8] at several overexpanded pressure ratios. Different turbulence models are assessed, and the inclusion of external flow is evaluated in terms of their effects on the predicted surface pressure distribution and nozzle thrust and flow coefficients.

### Computational Details

The NPARC Code [11] 2.0 was used to obtain the numerical solution to the two dimensional Reynolds averaged, compressible Navier-Stokes equations in strong conservation law form and general curvilinear coordinates. The code uses Pulliam's diagonalized Beam and Warming central difference time marching scheme with fully implicit second and fourth order artificial dissipation.

The flow is computed in the lower half of the nozzle, with symmetry boundary conditions at the upper boundary, and no slip boundary conditions at the nozzle wall. The total pressure and temperature are specified at the inflow boundary and the primitive variables are extrapolated for the outflow at the exit plane. The extrapolated quantities are the primitive variables used by the code. A characteristic scheme was implemented and applied at the exit boundary regions with reversed flow. The pressure is still specified at these regions, but the extrapolated quantities are the Riemann invariants. This method has been found to improve accuracy and robustness of the numerical solution.

Starting from uniform initial conditions corresponding to one dimensional subsonic flow at the nozzle inlet, the numerical solution was advanced using local time stepping as dictated by the maximum allowable CFL number. The convergence criteria was based on the variation in the thrust coefficients reaching less than 0.1%, which corresponded to 3 to 4 orders of magnitude reductions in the total L2 residual depending on the NPR.

### Results and Discussion

Figure 1 demonstrates geometric characteristics of nozzle configurations B2 and C2 whose design pressure ratio is equal to 8.8. Experimental results for these two nozzle configurations were reported in references [7] and [8]. The results consisted of static pressure distributions over the centerlines of the flaps and side walls, and flow and thrust coefficients at design and several overexpanded flow conditions. Nozzle configuration C2 at nozzle pressure ratio (NPR) = 2.4

was selected as the baseline to demonstrate grid independence, convergence history, and turbulence model effects.

### Grid Independence

A grid refinement study was conducted for the numerical solution obtained using the k- $\epsilon$  turbulence model in nozzle C2 at 2.41 NPR. Figure 3 shows the computational results obtained using the 161x68 grid of Fig. 2 and a coarser (81x34) grid with half the number of grid points in each direction together with the experimental data [8] for the static pressure distribution at the center of the flap. The value of  $Y^+$  for the first grid from the nozzle wall at the throat was equal to one for both grids. According to Fig. 3, the solutions for the two grids are very close except for a slight pressure oscillation after the shock in the coarse grid predictions. One can also see that the pressure level and the distance of the separation point from the throat are slightly over predicted in both cases. The rest of the computations were conducted using the 161x68 grid shown in Fig. 2.

### Turbulence Model Effects

The effect of the turbulence closure model on the performance prediction was studied using the baseline case (nozzle C2 at NPR = 2.41). Figure 4 presents the computed surface pressure distribution using three different turbulence models: Baldwin-Lomax [12], Baldwin-Barth [13] and Chien k- $\epsilon$  [14]. The surface pressure distribution shown in Fig. 4 indicates that there is a significant spread in the predicted shock location depending on the turbulence model used. Chien's k- $\epsilon$  model gives the closest agreement with the experimental results, while the Baldwin-Lomax and Baldwin-Barth models predict the shock to be respectively downstream and upstream of the experimental location. The predicted static pressure distributions downstream of shock are generally higher than the experimental results. Furthermore, the predicted pressure distributions after the shock, contain overshoots in the case of the algebraic and one equation turbulence models that are not observed experimentally.

The predicted nozzle performance parameters are shown in Table 1. The computed thrust coefficient using Baldwin-Barth and Chien k- $\epsilon$  turbulence models is higher than the experimental value due to the overprediction of the pressure level on the divergent flap of the nozzle behind the shock. Despite the fact that the pressure distribution predicted using the Baldwin-Lomax model exhibits the largest deviation from the experimental results, the thrust coefficient predicted by this model is closest to the experimental

value. However, the agreement is fortuitous as a result of the effects of predicting the shock location further downstream, canceling those associated with the pressure overprediction between the shock and the nozzle exit. Chien's  $k-\epsilon$  model is used in the rest of this study since it gave the best overall agreement with the experimental results for the pressure distribution.

### Flow Characteristics

The computed velocity vectors, Mach number and pressure contours for the base line case (nozzle C2 at NPR = 2.41) are presented in Figs. 5, 6 and 7. These figures indicate a normal shock with a large well defined lambda foot. The leading branch of the lambda shock extends to the nozzle surface while the trailing branch extends only to the detached shear layer. This indicates that the flow separates at the leading lambda foot and remains detached to the nozzle exit. Figure 8 presents a comparison between the computed shock structure and that deduced from the Schlieren photographs of ref. [8] in terms of the lambda shock angles and the extent of the normal shock at the center for the baseline case.

### Effect of Nozzle Pressure Ratio

Figure 9 compares the computed flap surface pressure distribution for nozzle C2 with the measured static pressures [8] along the centerline and at 20% of the nozzle half width from the end wall for five over expanded nozzle flow conditions. One can see closer agreement with the experimental results at the higher pressure ratios of 4.1, 3.4 and 2.4. Below NPR = 2.4, noticeable differences can be seen between the measured static pressures at the two flap locations indicating that the flow was three dimensional and the shock was non planar. The computational and experimental results are very close above NPR = 3.0, where two dimensional flow conditions in the experimental results, are reflected in the agreement between the pressure measurements at the two flap locations. Similar trends are observed in the case of B2 nozzle configuration for which the computational results at NPR = 2.95 and 1.96 are presented and compared with the experimental results of reference [7] in Fig. 10. A three dimensional flow simulation was conducted in nozzle C2 to study these effects and the results are reported in ref. [15].

### External Flow Effects

While the calculated shock position generally compared well with experiment, the pressure plateau after the shock was always higher than the experiment. A close examination of the experimental results of

reference [7] reveals that the wall pressure near the exit is lower than ambient, indicating a possible interaction between the flow in the recirculation region inside the nozzle and the surrounding air. In order to investigate the effects of this phenomenon on the pressure inside the nozzle, further numerical simulations were conducted including an external surrounding region in the computational domain.

Referring to Fig. 11, a grid that extends outside the nozzle was generated for the B2 configuration and two cases were run for nozzle pressure ratios of 1.96 and 2.95. The lateral boundary of the external flow region was at  $1.5 h_c$  and it extended  $3 h_c$  downstream and  $2.0 h_c$  upstream of the nozzle exit. Ambient conditions were specified for the total pressure and temperature at the external flow's upstream boundary and the primary variables were extrapolated at the lateral free boundaries. A two block grid, consisting of (235x68) internal and (128x56) external points was used in the computations (Fig. 11). Figure 10 compares the computed surface pressure with that obtained with the internal flow only. The results indicate that in general the inclusion of the external flow moves the shock locations slightly downstream and reduces the pressure plateau after the shock. The interaction with the external flow in the low NPR case causes 3.5% reduction in the pressure on the flaps near the exit, yet the overall agreement with the experimental results does not improve significantly. The streamlines shown in Fig. 12 reveal the nature of the interaction associated with the external flow entrainment into the nozzle's recirculation region. The high streamline curvature near the exit causes the computed reduction in the predicted flap pressure when the external flow is included.

### Performance Prediction

The calculated thrust and discharge coefficients are compared with the experimental values in Figs. 13 and 14 for nozzle configurations C2 and B2. One can see that the predicted discharge coefficients for the B2 cases are in excellent agreement with the experimental results. The differences observed in the C2 case are the result of a peculiarity in the experimental set-up. According to Hunter [8], the buckling of the transparent nozzle sidewalls in his experiment, and the associated change in the throat area produced erroneous variations in the discharge coefficient causing augmentation at high NPR's and reductions at low NPR's.

The agreement between the computational and experimental results for the thrust coefficient is less satisfactory as can be seen in Figs. 13 and 14. The

thrust coefficient predictions are in agreement with the experimental data for nozzle pressure ratios above 2.4 in both configurations. The differences increase as the NPR decreases, but remain below 4% in all cases except in the case of nozzle  $C_2$  at  $NPR = 1.8$ , where the difference reaches 8%. This difference is expected in view of three dimensional flow in the experiments at nozzle pressure ratios below 2.4.

### Conclusions

A numerical investigation was conducted to assess the accuracy with which the performance of an overexpanded two-dimensional convergent divergent nozzle can be predicted. Three turbulence models were compared and it was concluded that a two equation  $k-\epsilon$  model is required to accurately predict the shock location. The computed pressure distributions and performance parameters were compared with the experimental results for two nozzle configurations at design and several overexpanded pressure ratios. The computed results were in excellent agreement with the experimental results in terms of the pressure distribution upstream of the shock, the shock location and the pressure gradient across the shock. The degree of overpredicting the pressure plateau downstream of the shock increased as the pressure ratio decreased, resulting in overpredicting the thrust coefficient. The error in predicting the thrust based on two dimensional flow simulations remains below 2% when the recirculating separated flow region extends over less than 25% of the divergent nozzle length ( $NPR > 3.0$ ), and exceeds 4% when the separated region is more than 50% of the length ( $NPR < 2.4$ ). Modeling the interaction between the internal and external flow by extending the computational domain outside the nozzle slightly improves the agreement with the experiment.

### Acknowledgement

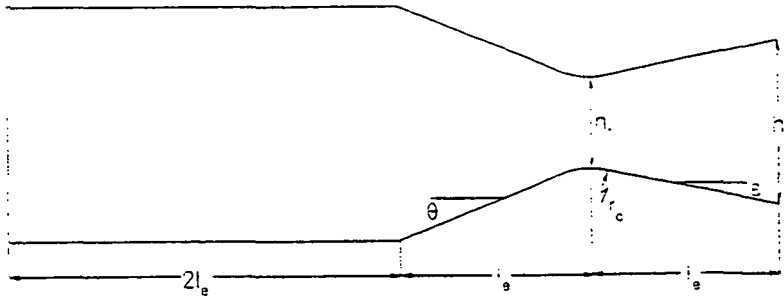
This work was sponsored by Ohio Aerospace Institute Subgrant No. 120520. The computational work was performed on the CRAY YMP of the Ohio Supercomputer Center.

### References

1. Dusa, D.J., "Exhaust Nozzle System Design Considerations for Turboramjet Propulsion Systems," ISOABE Ninth International Symposium on Air Breathing Engines, Athens, Greece, September 1989.
2. Ying, S.X., Bobba, C.R., and Youngmans, J.L., "Design and Performance Evaluation of Novel Exhaust Systems--A Numerical Study," Tenth International Symposium on Air Breathing Engines, September, 1991, Nottingham, UK, pp. 1085-1089.
3. Luffy, R.J., Hamed, A., "A Study on the Impact of Shroud Geometry on Ejector Pumping Performance," *AIAA Paper*, No. 92-3160, July, 1992.
4. Barker, T.J. and Anderson, O.L., "An Analytical Study of a Supersonic Mixer-Ejector Exhaust System," *AIAA Paper*, No. 91-0126, Jan. 1991.
5. Bobba, C.R., Rowe, R.K., Rout, R.K. and Kenkatapathy, E., "Computational Analysis of a 2DCD Nozzle Flow with the FL3D Solver," *AIAA Paper*, No. 94-0019, January, 1994.
6. Welterzlen, T.J., Catt, J.A. and Reno, J.M., "Evaluating F-16 Nozzle Drag Using Computational Fluid Dynamics," *AIAA Paper*, No. 94-0022, January, 1994.
7. Mason, M.L., Putnam, L.E., and Re, R.J., "The Effect of Throat Contouring on Two-Dimensional Converging-Diverging Nozzles at Static Conditions," NASA TP 1704, August, 1980.
8. Hunter, C.A., "An Experimental Analysis of Passive Shock-Boundary Layer Interaction Control for Improving the Off-Design Performance of Jet Exhaust Nozzles, M.S. Thesis, George Washington Univ., September 1993.
9. Shieh, Fang Shih, "Navier-Stokes Solutions of Transonic Nozzle Flow with Shock Induced Flow Separations," *Journal of Propulsion and Power*, Vol. 8, No. 4, July-August 1992, pp. 829-835.
10. Hamed, A., "An Investigation of Oblique Shock/Boundary Layer Interaction Control," AFOSR Technical Report Contract No. 91-0101, January, 1992.
11. Cooper, G.K. and Sirbaugh, J.R., "PARC Code: Theory and Usage," AEDC-TR-89-15, 1989.
12. Baldwin, B.S., Lomax, H., "Thin Layer Approximation and Algebraic Model for Separated Turbulent Flows," *AIAA Paper* 78-257, January 1978.
13. Baldwin, B.S., Barth, T.J., "A One-Equation Turbulence Transport Model for High Reynolds Number Wall-Bounded Flows," NASA-TM-102847, August 1990, N91-10252.
14. Chien, K-Y, "Prediction of Channel and Boundary-Layer Flows with a Low Reynolds Number Turbulence Model," *AIAA Journal*, Vol. 20, January 1982, pp. 33-38.
15. Hamed, A., Vogiatzis, C., "Simulations of Overexpanded 2DCD Nozzle Flows," *AIAA Paper* No. 95-2615, July 1995.

	Experiment	Chien k-ε	Baldwin-Barth	Baldwin-Lomax
Thrust Coefficient	0.904	0.927	0.941	0.898
Discharge Coefficient	0.979	0.988	0.988	0.988

Table I. Nozzle C2 at 2.41 NPR. Performance parameters for different turbulence models.



	B2	C2
$h_e$ (in)	1.94	1.94
$h_t$ (in)	1.08	1.08
$r_c$ (in)	1.08	0.63
$\theta$ (deg)	22.3	27.3
$\epsilon$ (deg)	11.2	11.0
$l_e$ (in)	2.28	2.28
$A_e/A_t$	1.80	1.80
$NPR_d$	8.81	8.81

Figure 1. Nozzle geometry.

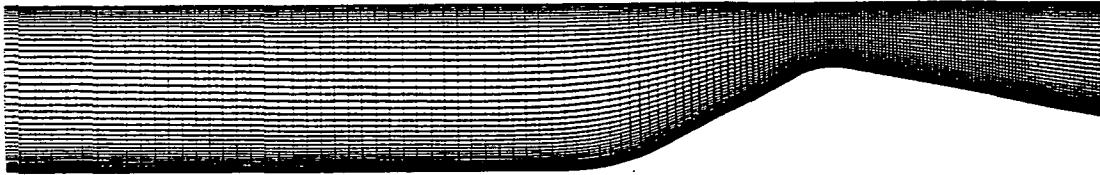


Figure 2. The thin grid (161x68) for the C2 nozzle.

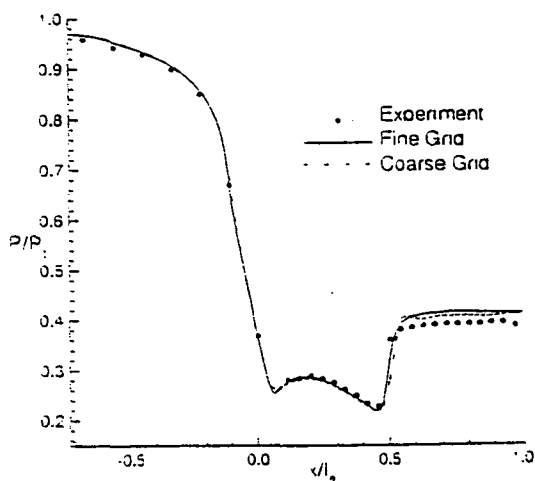


Figure 3. Flap pressure distributions for different grids (C2 nozzle at 2.41 NPR).

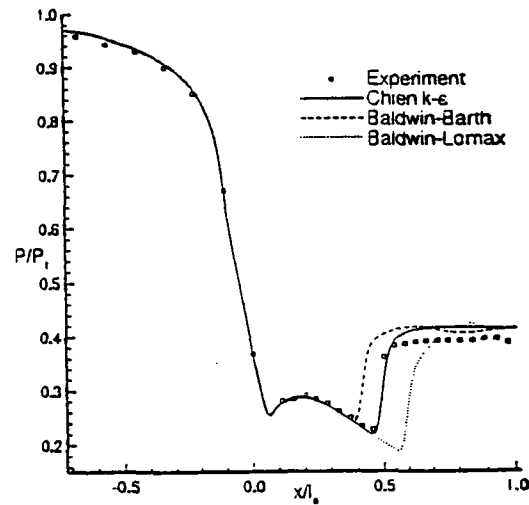
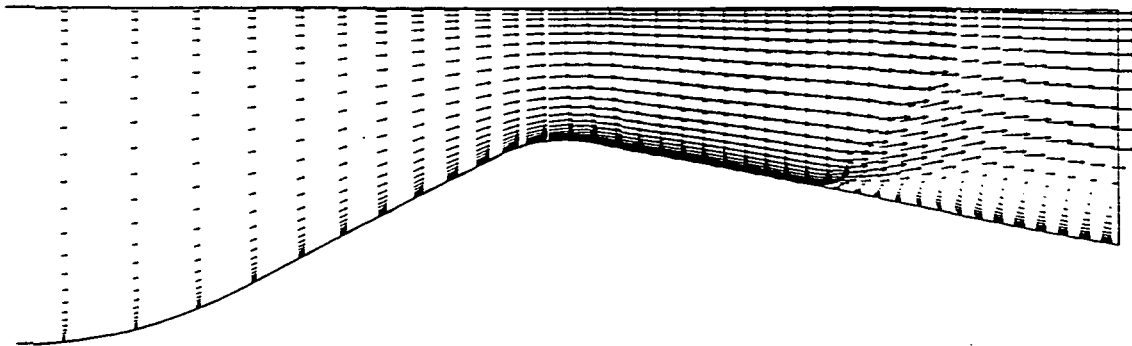
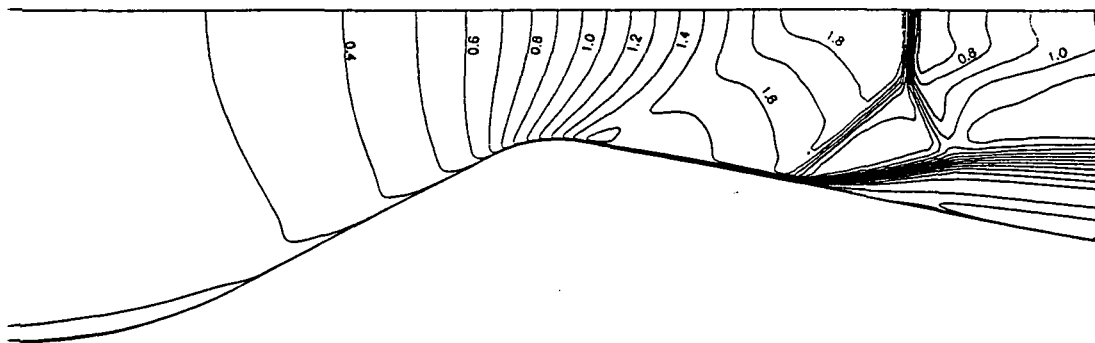


Figure 4. Flap pressure distributions for different turbulence models.



**Figure 5.** Velocity vectors for the baseline case (C2 nozzle at 2.41 NPR).



**Figure 6.** Mach number contours for the baseline case (C2 nozzle at 2.41 NPR).

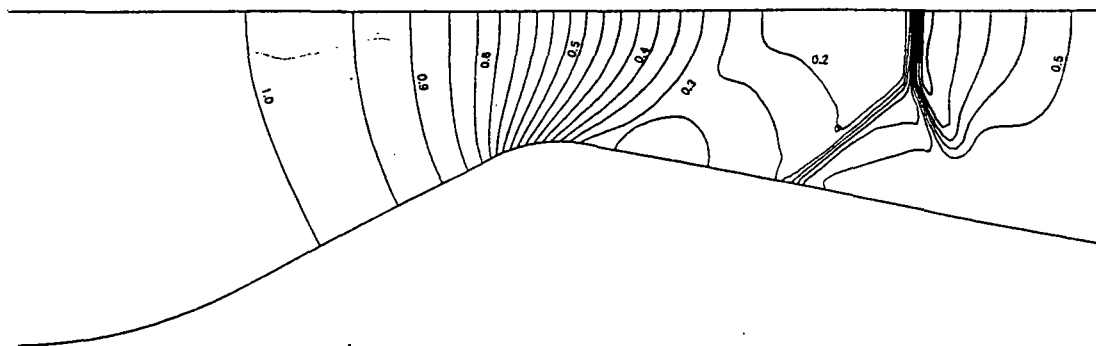


**Figure 7.** Pressure contours for the baseline case (C2 nozzle for 2.41 NPR).

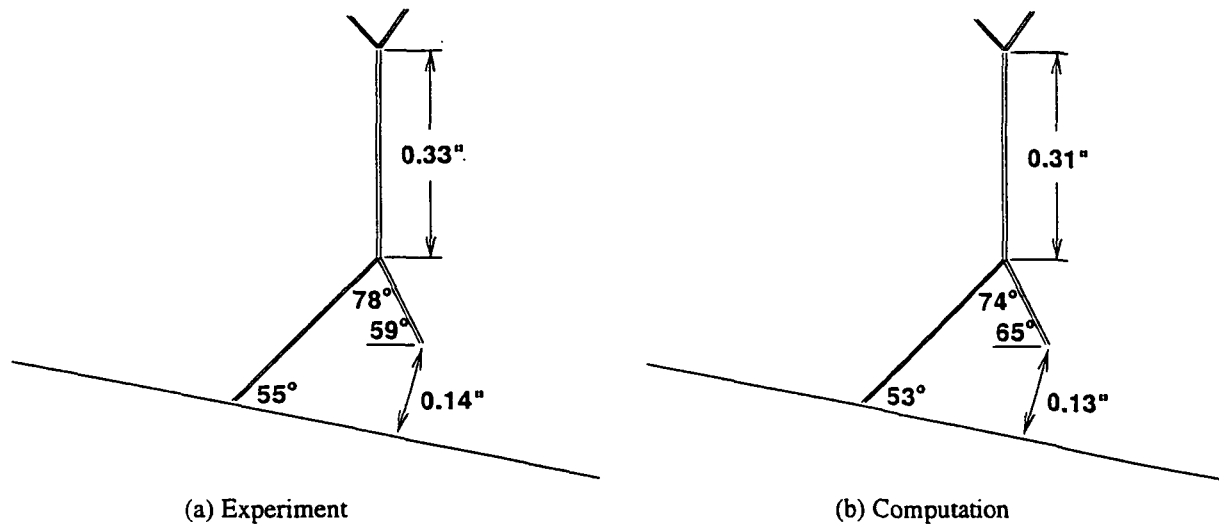


Figure 8. The shock structure for the C2 nozzle at 2.41 NPR.

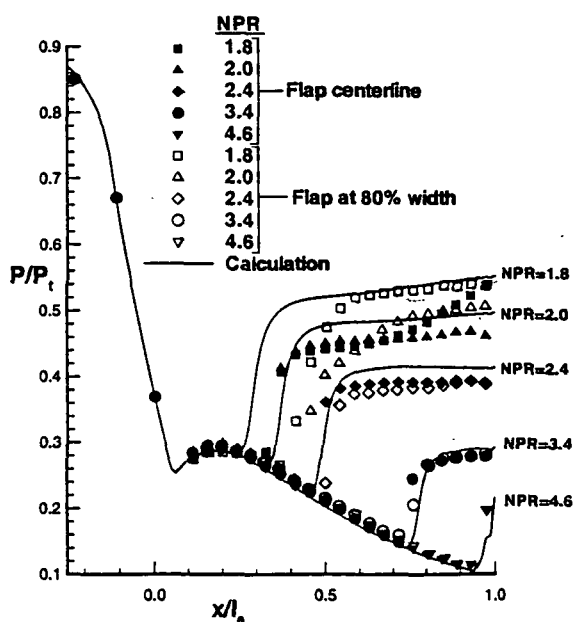


Figure 9. Surface pressure distributions for the C2 nozzle at different NPR's.

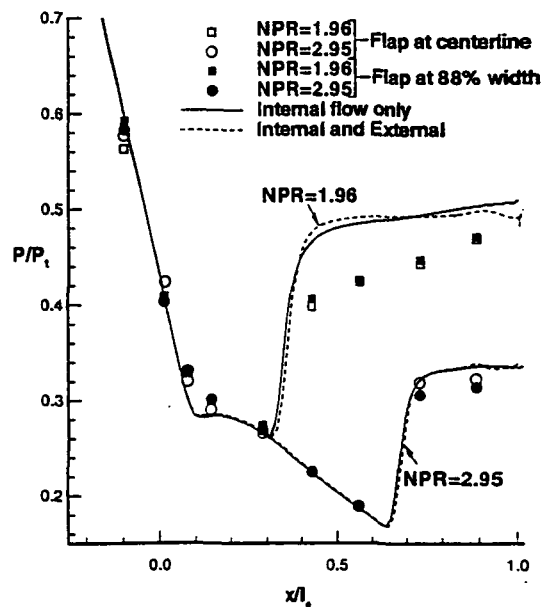


Figure 10. Surface pressure distributions at the middle of the flap for the B2 nozzle at different NPR's

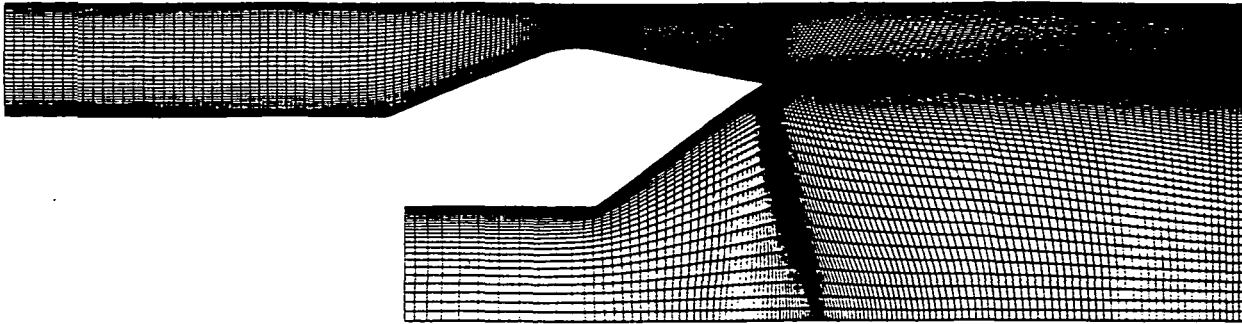


Figure 11. The internal-external flow grid for the B2 nozzle.

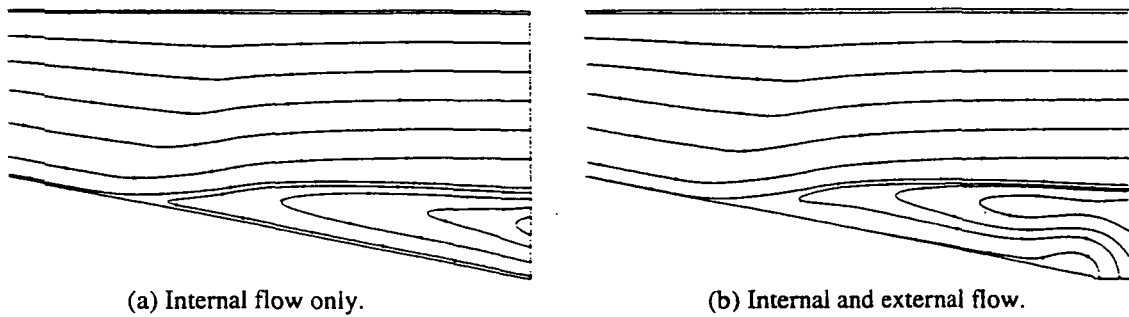


Figure 12. Streamlines for the B2 nozzle at 1.96 NPR.

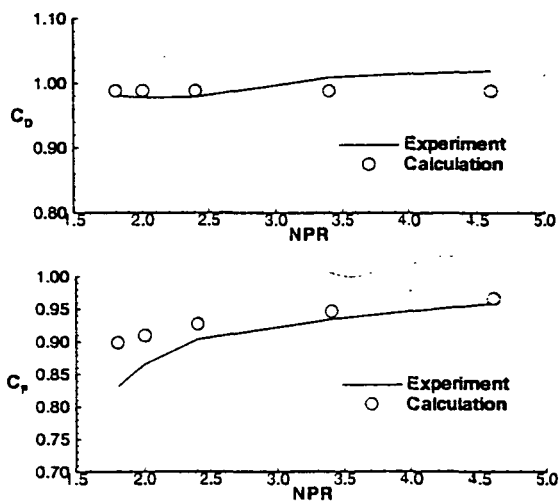


Figure 13. Performance predictions for the C2 nozzle.

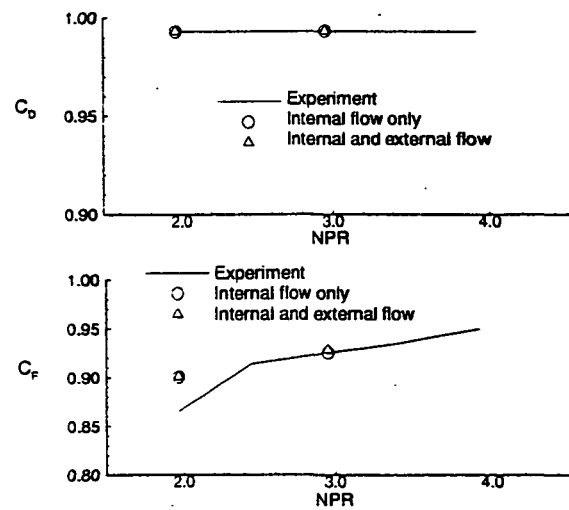


Figure 14. Performance predictions for the B2 nozzle.

**APPENDIX B**



**AIAA 95-2615**

**Assessment of Turbulence Models in  
Overexpanded 2D-CD Nozzle Flow Simulations**

**A. Hamed and C. Vogiatzis**

**University of Cincinnati**

**Cincinnati, OH**

**31st AIAA/ASME/SAE/ASEE  
Joint Propulsion Conference and Exhibit  
July 10-12, 1995/San Diego, CA**

# ASSESSMENT OF TURBULENCE MODELS IN OVEREXPANDED 2D-CD NOZZLE FLOW SIMULATIONS

A. Hamed<sup>\*</sup> and C. Vogiatzis<sup>\*\*</sup>  
University of Cincinnati  
Cincinnati, OH 45221

## Abstract

An investigation was conducted to assess the performance of different turbulence models in the numerical simulations of two dimensional convergent divergent (2DCD) nozzle flow fields at overexpanded conditions. The implicit numerical solution of the compressible two dimensional Navier-Stoke equations was obtained using the NPARC code. Five different turbulence closure models were used in the computations and the results compared to existing experimental data at design and overexpanded conditions. The results indicate little differences among the predictions using the algebraic, one equation, and two equation turbulence models at design pressure ratio. However large differences in the predicted shock location and pressure level behind the shock were observed at overexpanded conditions. The two equation  $k-\epsilon$  and  $k-\omega$  turbulence models, gave the best overall agreement with the experimental measurements for thrust and static pressure distribution over the flaps. The agreement deteriorates with decreased nozzle pressure ratio (NPR) as the shock moves upstream and three dimensional flow effects increase downstream.

## Introduction

There is renewed interest in 2D-CD nozzles because of the advantages they offer over axisymmetric configurations for supersonic transport. These include higher performance, reduced afterbody drag, easier integration with airframes, and large mechanical area excursion capabilities. It is well known that the take off gross weight is very sensitive to nozzle performance at cruise flight conditions<sup>1</sup>, and that high area ratios are required for best efficiency at supersonic cruise. The performance of these nozzles can suffer at off design conditions when the large nozzle area ratio reductions required during subsonic and transonic acceleration, cannot be achieved under the mechanical and control system constraints. Since this can adversely affect the acceleration time to cruise, the fuel burnt and range, it is desirable to predict off design performance with a high degree of accuracy.

Very few experimental studies report detailed measurements in overexpanded 2D-CD nozzles. Mason et al<sup>2</sup> presented internal performance data for five 2D-CD nozzle geometries tested in the static test facility of Langley's 16-ft transonic tunnel. Hunter<sup>3</sup> tested another 2D-CD nozzle configuration in the same facility and reported experimental data for the internal thrust and discharge coefficients, and static pressure distribution over the flap at different NPRs.

Overexpanded nozzle predictions are complicated by the large shock induced separated flow regions in the divergent nozzle section. Gerard et al<sup>4</sup> and Shieh<sup>5</sup> presented computational results at one overexpanded condition, and compared only the static pressure distribution with the experimental data of Mason et al<sup>2</sup>. Hamed et al<sup>6</sup> presented computational results at several overexpanded flow conditions for two 2D-CD nozzle configurations tested by Mason<sup>2</sup> and Hunter<sup>3</sup>. They also modeled the interactions with the external flow by extending the solution domain outside the nozzle. The purpose of the present investigation is to assess the computational results obtained using five different turbulence models in terms of the convergence characteristics and the agreement of the computed pressure distribution and thrust coefficient with the experimental data in overexpanded 2D-CD nozzles.

## 2D-CD nozzle. Configuration and operating conditions.

The 2D-CD nozzle tested by Hunter<sup>3</sup> in Langley's static test facility was selected for the numerical assessment because the large number of pressure taps gave a better definition of the shock location. The nozzle has a design pressure ratio of 8.8 for an exit Mach number of 2.1. The convergent nozzle section's area ratio is 2.56 and its convergence angle 22.3°, while the divergent nozzle section's area ratio is 1.796 and its divergence angle 11.2°. The distance between the side walls is approximately 4.1 times the throat height of 1.08 inches, and the throat radius of curvature is  $r_c=0.625$  inches. The nozzle was tested at design and several overexpanded flow conditions for NPR's ranging between 1.255 and 8.8. The experimental results<sup>3</sup> consist of flow and thrust

<sup>\*</sup>Professor, Fellow AIAA

<sup>\*\*</sup>Student Member AIAA

Copyright (c) 1995 by the American Institute of Aeronautics and

coefficients, as well as static pressure distribution over the flaps at the centerline, and at 10% of the nozzle width from the endwalls. In addition Schlieren photographs were also presented showing the location and structure of the shock in the divergent nozzle section.

### Computations

#### Flow Solver and Boundary Conditions

The NPARC code<sup>7</sup> was used to obtain the numerical solution to the compressible two dimensional Navier-Stokes equations on Cray Y-MP. The code is based on the use of the approximate factorization scheme of Beam-Warming in the solution of the time dependent, Reynolds averaged Navier-Stokes equations in conservation law form and general curvilinear coordinates. The computations were performed using five different turbulence models, namely Baldwin-Lomax and RNG algebraic models, Baldwin-Barth one equation model, and the two equation  $k-\epsilon$  and  $k-\omega$  turbulence models of Chien<sup>8</sup> and Wilcox<sup>9</sup> respectively. The first four turbulence models exist in NPARC-2.0. The last was implemented in NPARC-2.1 by Yoder and Georgiadis<sup>10</sup>. The flow is computed in the lower half of the nozzle, with symmetry boundary conditions at the upper boundary, and no slip adiabatic boundary conditions over the flap. Free boundary conditions were applied at the nozzle inlet and exit.

#### Computational Grid

Referring to figure 1, a one block 161x68 grid, was generated in the lower half of the nozzle using an elliptic grid generator (GRIDGEN<sup>11</sup>), with half the grid points in the divergent part of the nozzle. The  $Y^+$  for the first grid point next to the wall was equal to 1.0 in the throat region, with at least 15 points inside the wall boundary layer.

This grid was selected after a grid refinement study was conducted at 2.41 nozzle pressure ratio. The results obtained using the 161x68 grid of figure 1 and a coarser (81x34) with the same value of  $Y^+$  for the first grid from the nozzle wall, were very close in predicting the pressure distribution before and after the shock, and differed only in the pressure gradient across the shock, which improved with grid refinement.

### Convergence

The solution was advanced using local time stepping and the maximum allowable CFL value. This varied from 2.0 for the high pressure ratio cases to 1.0-1.5 for the low pressure ratios. The nozzle thrust and flow coefficients were computed and monitored during the iterations. The internal thrust coefficient was determined from the integration of the axial momentum at the exit plane, and the flow coefficient, from the integration of the mass flux at several normal planes upstream of the throat. A variation of less than 0.1% in thrust or mass flow over 1000 iterations was required, to consider the solution converged. Additional iterations were sometimes required to converge the nozzle performance parameters, after the residual information indicated convergence, typically 2 to 4 orders of magnitude reduction. Conversely small flow regions sometimes kept the numerical residuals from further reductions after the nozzle performance parameters have converged. Weterlen et al<sup>12</sup> reported similar behavior in their numerical computations of nozzle drag.

### Results And Discussions

Computational results are presented and compared with the experimental data of Hunter<sup>3</sup> over a range of nozzle pressure ratios corresponding to design and several overexpanded conditions.

#### Predictions at the design pressure ratio

The convergence characteristics of the numerical solution obtained using the different turbulence models at design pressure ratio are shown in figure 2. In all cases the numerical solution was advanced using local time stepping from uniform initial conditions corresponding to one dimensional subsonic flow at the nozzle inlet. The maximum CFL number for these cases was found to be equal to 2.0. The algebraic turbulence models were used from the beginning of the calculation. For the one and two equation models, the turbulence viscosity field was initialized using Baldwin-Lomax turbulence model for 2000 iterations. According to figure 2 the residuals are reduced three orders of magnitude within 5,000 iterations and another order of magnitude over the next 5,000 iterations in all cases but the RNG turbulence model, where it does not decrease below two orders of magnitude.

The computed pressure distributions for the different turbulence models are shown in figure 3. The

curves practically coincide and the agreement with the experiment is excellent. A comparison of the computed nozzle performance predictions for the five turbulence models at design conditions is summarized in table 1. According to this data, the thrust coefficient was predicted within 0.8% of the experimental results in all cases except for the RNG model where the predictions were within 1.0%.

#### Predictions at overexpanded conditions

The computations of the nozzle flow field were performed using the five turbulence models at one overexpanded condition corresponding to a nozzle pressure ratio 2.41 ( 27% of design value ). From the convergence history shown in figure 4, it is obvious that the total residual decrease is approximately two orders of magnitude smaller than the design pressure ratio case. This is attributed to the massive shock induced flow separation, which occupies over 60% of the divergent nozzle length and 30 % of the exit width. The typical thrust coefficient evolution presented in figure 5 indicates that variation of less than 0.1% are reached after 10,000 iterations.

Typical Mach number and turbulence viscosity contours and velocity vectors, are presented in figures 7a, 7b and 7c. These results, which were obtained using the  $k-\omega$  model, indicate a normal shock with a large well defined lambda foot. The leading branch of the lambda shock extends to the nozzle surface, where the flow separates and remains detached to the nozzle exit. The highest turbulence viscosity levels are predicted in the separated flow region behind the shock.

The surface pressure distributions shown in figure 7 indicate that there is a significant spread, of about 40% of the throat opening in the predicted shock location, depending on the turbulence model used. At this pressure ratio Wilcox's  $k-\omega$  model was the closest to the experimental results in predicting the pressure variation behind the shock, but Chien's  $k-\epsilon$  model was closer in predicting the shock location. The algebraic and one equation models predicted shock positions respectively upstream and downstream of the experimental location. Furthermore, their predicted post shock pressures were higher, and contained overshoots not observed experimentally.

The computed exit velocity profiles using the different turbulence models are compared in figure 8. The results indicate that the shear layer is independent

of the turbulence model in spite of the difference in the predicted shock location. The predictions using the one equation turbulence model of Baldwin-Barth exhibited the largest velocities in the supersonic region above, and the reversed flow region below the shear layer. Conversely the predictions using the algebraic turbulence models exhibited the lowest velocities in both these regions. The predicted velocities were very close in the core transonic region, with the highest values predicted by the  $k-\omega$  model and the lowest by the algebraic models.

The corresponding thrust coefficients are compared with the experimental results in table 2. The computed thrust coefficients using all the turbulence models with the exception of Baldwin-Lomax are higher than the experimental value. Despite the fact that the pressure distribution predicted using the algebraic turbulence models (Baldwin-Lomax and RNG) exhibited the largest deviation from the experimental results, the thrust coefficients predicted by these models are fortuitously closest to the experimental value.

Further numerical solutions were obtained with the two equation turbulence models over a number of overexpanded pressure ratios. Figure 9 and figure 10 compare the computed static pressure distribution over the flap to the experimental results of Hunter<sup>3</sup> at the centerline and near the end walls. Satisfactory agreement with the experimental results is observed at nozzle pressure ratios above 2.41. The three dimensional effects downstream of the shock increase below this pressure ratio as indicated by the differences between the static pressure at the centerline and the flap end wall. Table 3 and figure 11 compare the computed thrust coefficient using the two equation turbulence models, with the experimental results at five different nozzle pressure ratios. The two equation turbulence model thrust coefficient predictions are within 1% of the experimental data for nozzle pressure ratios above 50% design, and within 2% above 30% design. Increased deviations at lower pressure ratios are attributed to three dimensional flow effects caused by the interactions between the shock and endwall boundary layers.

#### Conclusions

An assessment of five turbulence models was conducted in a 2DCD nozzle at different operating conditions. The two dimensional flow field solutions using the NPARC code were required to meet several

convergence criteria including the nozzle flow and thrust coefficients. The turbulence models considered are the algebraic models of Baldwin-Lomax, RNG, the one equation model of Baldwin-Barth and the two equation  $k-\epsilon$  and  $k-\omega$  models of Chien and Wilcox. All five turbulence models yielded essentially identical solutions at design points and correlated well with the experimental pressure distribution over the flaps. The internal thrust coefficient predictions were within 0.8% of the experimental data under these conditions in all cases but the RNG model.

At overexpanded conditions agreements among the different models and with the experimental data prevailed only up to the point of shock induced flow separation and then varied significantly in the predicted shock location and pressure level behind the shock. The algebraic turbulence models predicted the shock location downstream of the experimental position, and the one equation model predicted the shock location upstream of the experimental position. Both overpredicted the pressure level behind the shock with overshoots not exhibited in the experimental pressure distribution. The two equation turbulence models gave the best Overall agreement with the experimental pressure distributions at overexpanded conditions. In spite of the massive flow separation, the thrust coefficient was predicted within 1.0% of the experimental values for nozzle pressure ratios above 50% design. Below these pressures, two dimensional flow predictions are inadequate because of the strong three dimensional flow effects behind the shock.

#### Acknowledgment

This work was sponsored by Ohio Aerospace Institute Subgrant No. 120520. The computational work was performed on the CRAY YMP of the Ohio Supercomputer Center

#### References

- <sup>1</sup> Shaw, R. J., Gilkey, S. and Hines, R. "Engine Technology Challenges for 21st Century High Speed Civil Transport" International Symposium on Air Breathing Engines, Tokyo, Japan, Sept. 20-24, 1993.
- <sup>2</sup> Mason, M.L., Putnam, L.E., and Re, R.J., "The Effect of Throat Contouring on Two-Dimensional Converging-Diverging Nozzles at Static Conditions," NASA TP 1704, August, 1980.
- <sup>3</sup> Hunter, C.A., "An Experimental Analysis of Passive Shock-Boundary Layer Interaction Control for Improving the Off-Design Performance of Jet Exhaust Nozzles, M.S. Thesis, George Washington Univ., September 1993.
- <sup>4</sup> Garrard, G., Phares W., Cooper G., "Calibration Of Parc for Propulsion Flows", AIAA/SAE/ASME/ASEE 27<sup>th</sup> Joint Propulsion Conference, June 24-26, 1991, Sacramento, CA
- <sup>5</sup> Shieh, Fang Shih, "Navier-Stokes Solutions of Transonic Nozzle Flow with Shock Induced Flow Separations," Journal of Propulsion and Power, Vol. 8, No. 4, July-August 1992, pp. 829-835
- <sup>6</sup> Hamed A., Vogiatzis C., Yeuon J.J., "Performance Prediction of Overexpanded 2D-CD Nozzles", 12<sup>th</sup> International Symposium on Air Breathing Engines, September 10-15, 1995, Melbourne, Australia
- Cooper, G.K. and Sirbaugh, J.R., "PARC Code: Theory and Usage," AEDC-TR-89-15, 1989.
- <sup>8</sup> Chien, K-Y, "Prediction of Channel and Boundary-Layer Flows with a Low Reynolds Number Turbulence Model," AIAA Journal, Vol. 20, January 1982, pp. 33-38.
- <sup>9</sup> Wilcox, D.D., "The Remarkable Ability of Turbulence Model Equations to Describe Transition", Fifth Symposium on Numerical and Physical Aspects of Aerodynamic Flows, California State University, Long Beach, California, 13-15 January 1992.
- <sup>10</sup> Yoder, D.A., Georgiadis N.J., "A User's Guide to NPARC k-w", Private Communication.
- <sup>11</sup> Steinbrenner, J.P., Chawner, J.R., and Fouts, C.L., "The GRIDGEN 3D Multiple Block Grid Generation System", WRDC-TR-90-3022 Vols. I and II, Wright-Patterson AFB, OH, 1990
- <sup>12</sup> Welterlen, T.J., Catt, J.A. and Reno, J.M., "Evaluating F-16 Nozzle Drag Using Computational Fluid Dynamics" AIAA 94-0022, Jan 1994.

ORIGINAL PAGE IS  
OF POOR QUALITY

	Experiment	Wilcox k- $\omega$	Chien k- $\epsilon$	Baldwin-Barth	Baldwin-Lomax	RNG
Thrust Coefficient	0.987	0.995	0.995	0.995	0.995	0.997
%error in thrust	-	0.8%	0.8%	0.8%	0.8%	1.0%

Table 1. Thrust coefficient at design pressure ratio (NPR=8.81).

	Experiment	Wilcox k- $\omega$	Chien k- $\epsilon$	Baldwin-Barth	Baldwin-Lomax	RNG
Thrust Coefficient	0.904	0.923	0.927	0.941	0.898	0.907
%error in thrust		2.1%	2.5%	4.1%	-0.7%	0.3%

Table 2. Thrust coefficient at NPR=2.41 (27% of design pressure ratio).

		NPR=2.0	NPR=2.4	NPR=3.4	NPR=4.6	NPR=8.8
Experiment		0.866	0.904	0.935	0.959	0.987
k- $\epsilon$	Thrust Coefficient	0.900	0.927	0.947	0.966	0.995
	%error in thrust	3.9%	2.5%	1.3%	0.7%	0.8%
k- $\omega$	Thrust Coefficient	0.911	0.923	0.952	0.971	0.995
	%error in thrust	5.2%	2.1%	1.8%	1.2%	0.8%

Table 3. Thrust coefficient at different pressure ratios

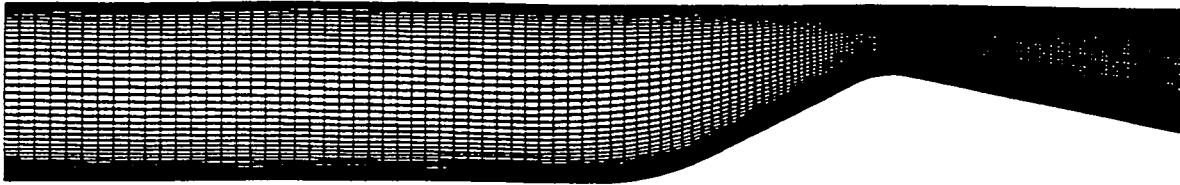


Figure 1. Computational grid (161x68).

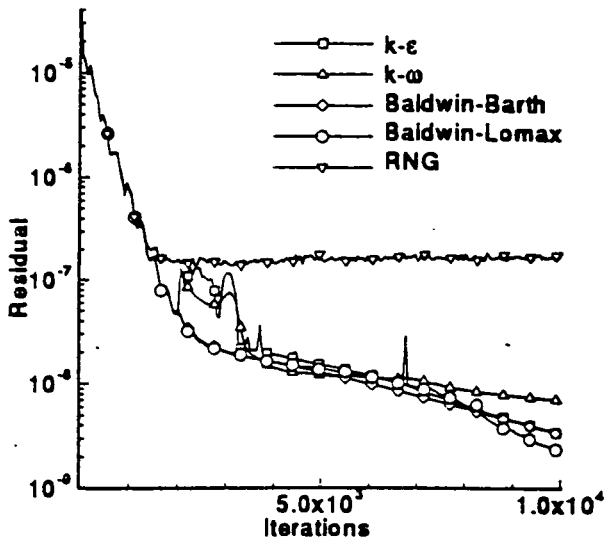


Figure 2. Convergence history at design pressure ratio (NPR=8.8).

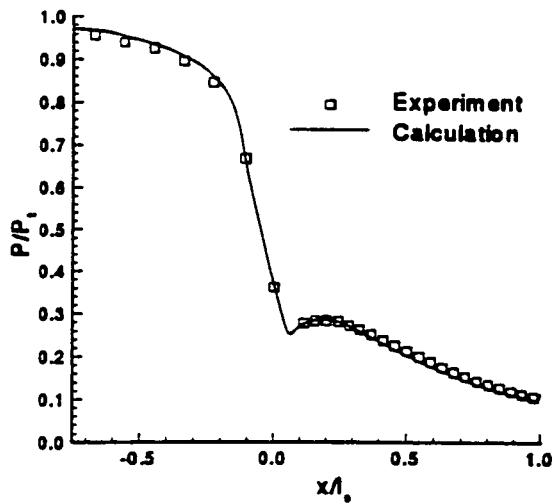


Figure 3. Surface pressure distribution at design pressure ratio (NPR=8.8).

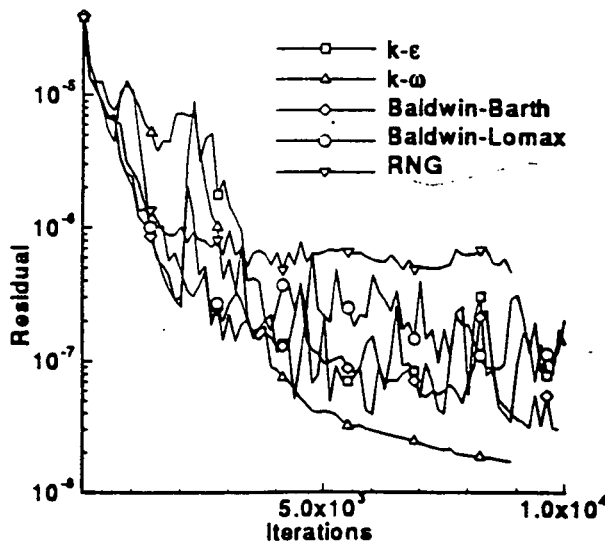


Figure 4. Convergence history (NPR=2.41)

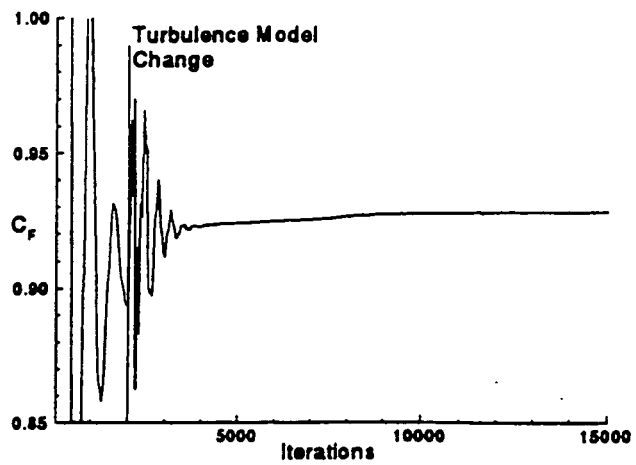
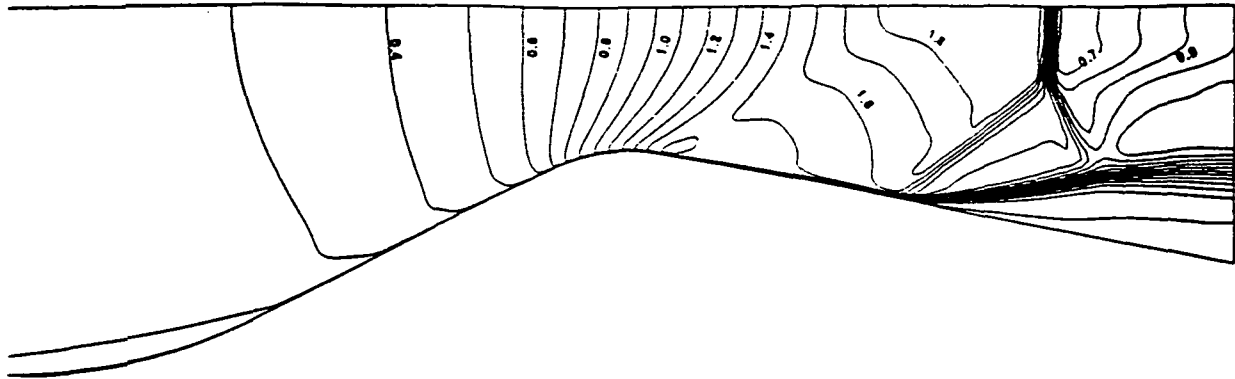
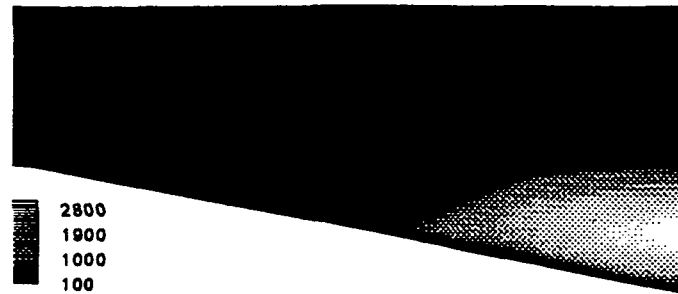


Figure 5. Thrust coefficient evolution (NPR=2.41).

ORIGINAL PAGE IS  
OF POOR QUALITY



**Figure 6a.** Mach number contours using the  $k-\omega$  turbulence model (NPR=2.41)



**Figure 6b.** Turbulence viscosity contours using the  $k-\omega$  turbulence model (NPR=2.41)

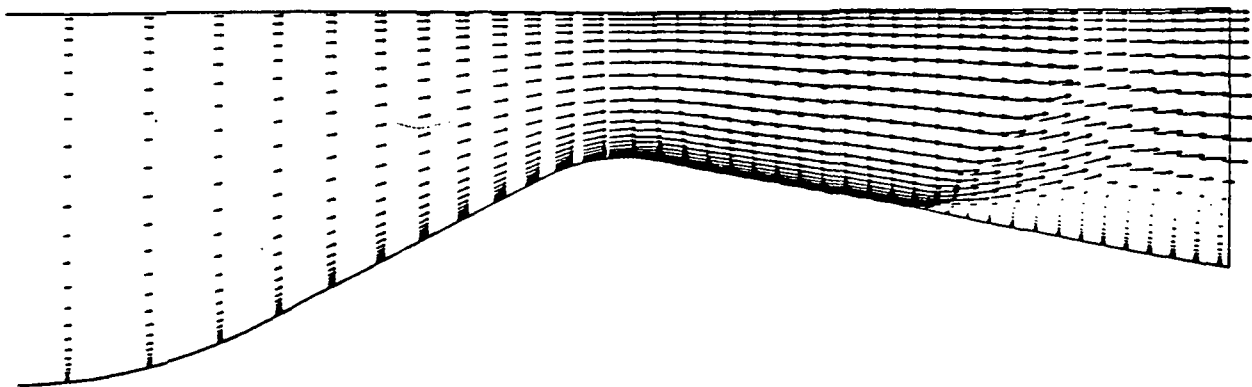


**Figure 6c** Velocity vectors using the  $k-\omega$  turbulence model (NPR=2.41)

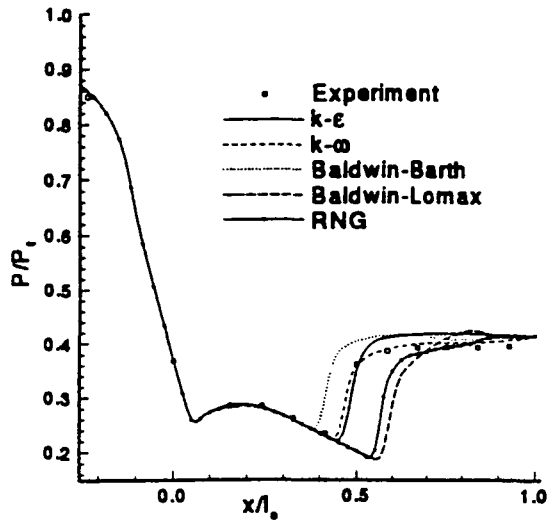


Figure 7. Surface pressure distributions (NPR=2.41).

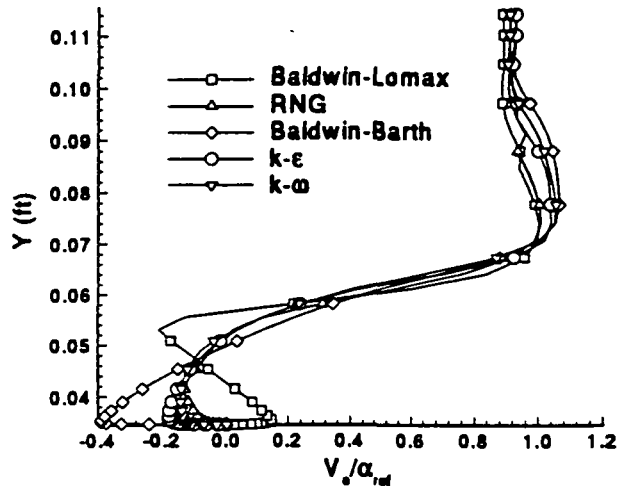


Figure 8. Exit velocity profiles (NPR=2.41)

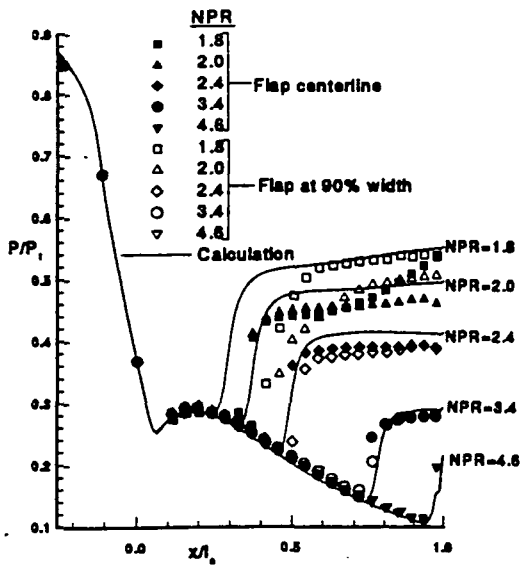


Figure 9. Surface pressure distribution using Chien's  $k-\epsilon$  turbulence model

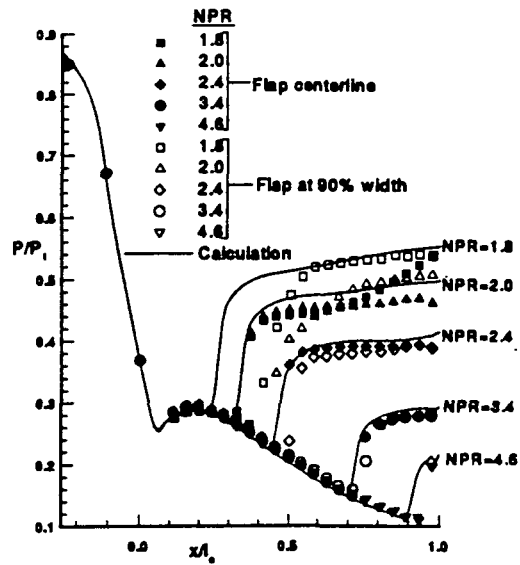


Figure 10 Surface pressure distribution using Wilcox's  $k-\omega$  turbulence model.

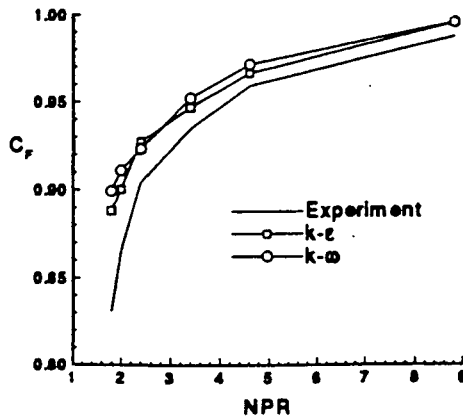


Figure 11 Thrust coefficient predictions